Timescales of motor memory formation in dual-adaptation

Abbreviated title: Timescales of motor memory formation in dual-adaptation

Marion Forano, David W. Franklin

Neuromuscular Diagnostics, Department of Sport and Health Sciences, Technical University of Munich,80992 Munich, Germany

Correspondence:
Dr. David Franklin
Neuromuscular Diagnostics, Department of Sport and Health Science, Technical University of Munich,
Campus D - Uptown München, Georg-Brauchle-Ring 60/62,
80992 Germany

Telephone: +49.89.289.24536
Email: david.franklin@tum.de

Number of pages: 45
Number of figures: 8
Number of words for Abstract: 248
Number of words for Introduction: 626
Number of words for Discussion: 1498

Acknowledgements: The authors declare no competing financial interests. We thank Justinas Česonis for helpful suggestions throughout this work.

Abstract

The timescales of adaptation to novel dynamics are well explained by a dual-rate model with slow and fast states. This model can predict interference, savings and spontaneous recovery, but cannot account for adaptation to multiple tasks, as each new task drives unlearning of the previously learned task. Nevertheless, in the presence of appropriate contextual cues, humans are able to adapt simultaneously to opposing dynamics. Consequently this model was expanded, suggesting that dual-adaptation occurs through a single fast process and multiple slow processes. However, such a model does not predict spontaneous recovery within dual-adaptation. Here we assess the existence of multiple fast processes by examining the presence of spontaneous recovery in two experimental variations of an A-B-Error-clamp paradigm within dual-task adaptation in humans. In both experiments, evidence for spontaneous recovery towards the initially learned dynamics (A) was found in the error-clamp phase, invalidating the one-fast-two-slow dual-rate model. However, as adaptation is not only constrained to two timescales, we fit twelve multi-rate models to the experimental data. BIC model comparison again supported the existence of two fast processes, but extended the timescales to include a third rate: the ultraslow process. Overall, we show that dual-adaptation can be best explained by a two-fast-triple-rate model over the timescales of adaptation studied here. Longer term learning may require even slower timescales, explaining why we never forget how to ride a bicycle. Indeed, even within our

single day experiment, we found little evidence for decay of the learned memory over several hundred error-clamp trials.

Significance Statement

Remembering motor skills is crucial to perform basic daily life tasks. However we still have limited understanding of the computational structure of these motor memories, an understanding that is critical for designing rehabilitation. Here we demonstrate that learning any task involves adaptation of independent fast, slow and ultraslow processes to build a motor memory. The selection of the appropriate motor memory is gated through a contextual cue. Together our work extends our understanding of the architecture of motor memories, by merging disparate computational theories to propose a new model.

Introduction

The generation of smooth and accurate movements requires predictive compensation of both internal and external dynamics, thought to arise through the formation of an internal model (Conditt et al., 1997; Wolpert et al., 1998; Kawato, 1999; Krakauer et al., 1999). This model, termed here a motor memory, is formed through repeated practice and driven by error and reward signals: a form of motor adaptation (Scheidt et al., 2000; Criscimagna-Hemminger et al., 2010; Izawa and Shadmehr, 2011; Trent and Ahmed, 2013; Herzfeld et al., 2014). Having been learnt, a motor memory can remain for months or years (Brashers-Krug et al., 1996; Smith et al., 2005). Similar to visuomotor (Krakauer et al., 2005) and saccadic

adaptation (Kojima et al., 2004), adaptation to novel dynamics exhibits savings (Medina et al., 2001; Caithness et al., 2004; Kojima et al., 2004), spontaneous recovery (Smith et al., 2006; Ethier et al., 2008) and interference (Karniel and Mussa-Ivaldi, 2002; Osu et al., 2004; Howard et al., 2013). This adaptation to novel dynamics has been shown to be well explained by a two-state model with different timescales (Smith et al., 2006). Within this framework, short-term motor memory is composed of one fast system that learns quickly but forgets quickly, and one slow system that learns slowly but retains more of the learning. Importantly, this architecture of motor memory is able to reproduce many aspects of motor adaptation, including interference and spontaneous recovery.

However, this two-state model cannot account for dual-adaptation, as introducing a new task drives the unlearning of the first task (Lee and Schweighofer, 2009). Studying dual-adaptation, that is learning simultaneously two opposing tasks, aims to explore the type of adjustments that might occur during everyday life. In daily life, we consistently switch between different tasks, going from drinking a cup of tea to controlling our computer mouse. As we change from one task to another, we need to adjust appropriately for the change in the dynamics of the external objects (cup) or sensorimotor transformations (to the computer screen). Like other single task models (Scheidt et al., 2000; Franklin et al., 2008), the dual-rate model (Smith et al., 2006) lacks the ability to represent and switch between different motor memories. In the absence of specific contextual cues, our sensorimotor system is also unable to learn two opposing dynamics over the same workspace; a phenomenon termed interference (Krakauer et al., 1999; Karniel and Mussa-Ivaldi, 2002; Smith et al., 2006). However when relevant contextual cues are provided, participants are able to simultaneously

adapt to opposing dynamics (Krakauer et al., 1999; Nozaki et al., 2006; Hirashima and Nozaki, 2012; Howard et al., 2013), indicating the formation of independent motor memories.

In order to integrate dual-adaptation, the dual-rate model was expanded to a single fast process and multiple slow processes gated by a binary cue representing the context (Lee and Schweighofer, 2009). This model proposes that these multiple slow processes act in parallel, forming a specific memory for each of the learned tasks. Within this model, interference between learning two opposing tasks is reduced, as the contextual cue gates a specific slow process, allowing only its modification, while avoiding alterations of other slow processes. However, this model (Lee and Schweighofer, 2009) claims that there is only a single fast process which adapts to any errors regardless of the contextual cue. When switching between tasks, this single fast process de-adapts to one while adapting to another, thereby not contributing to the formation of distinct motor memories. However, here we propose that a structure with a single fast process and multiple slow processes does not predict the existence of spontaneous recovery within a dual-adaptation paradigm. Therefore, we directly test the proposed model by examining the presence or absence of spontaneous recovery during simultaneous adaptation to two opposing force fields.

Materials and Methods

Participants

Twenty-three force field naive participants with no known neurological disorders participated in two experiments. Three participants (one of experiment 1 and two of experiment 2) were removed for further analysis as they were not able to simultaneously adapt to the two force

fields. In total 10 participants data was analyzed for both experiment 1 (n = 10, 7 female, 5 male, age 28±2.8 years) and experiment 2 (n = 10, 7 female, 5 male, age 28±2.8 years). All participants were right-handed based on the Edinburgh handedness questionnaire (Oldfield, 1971), and provided written informed consent before participating. The Ethics Committee of the Medical Faculty of the Technical University of Munich approved the study.

Apparatus

Participants grasped the endpoint handle of a vBOT planar robotic manipulandum and virtual reality system (Howard et al., 2009), with their forearms supported against gravity using an air sled. The participants were seated in a custom adjustable chair in front of the apparatus, strapped with a four-point seat belt to reduce body movement. The vBOT system is a custom built robotic interface that can apply state-dependent forces on the handle while recording the position and velocity in the planar workspace (Figure 1D). This horizontal plane was located approximately 15 cm below the shoulder. A six-axis force transducer (ATI Nano 25; ATI Industrial Automation) measured the end-point forces applied by the participant on the handle. Joint position sensors (58SA; Industrial encoders design) on the motor axes were used to calculate the position of the vBOT handle. Position and force data were sampled at 1kHz. Visual feedback to the participants was provided horizontally from a computer monitor fixed above the plane of movement and reflected via a mirror system that prevented visual feedback of the participants' arm. The visual feedback, provided in the same plane as the movement, consisted of circles indicating the start, target and cursor positions on a black background.

Protocol

Participants initiated a trial by moving the cursor representing the hand position (red circle of 1.0 cm diameter) into the start position (grey circle of 1.5 cm diameter) located approximately 20 cm directly in front of the participant. This start position turned from grey to white once the cursor entered it. Once the hand was within the start position for a random time between 1 and 2s, a go-cue (short beep) was provided signaling participants to initiate a reaching movement to the target (yellow circle of 1.5 cm diameter). The target was located 20.0 cm directly in front of the start position. The movement was considered complete when the participants maintained the cursor within the target for 600ms. After each trial, the participant's hand was passively driven to the start position while the visual feedback regarding the success of the previous trial was provided. Successful trials were defined as trials that did not overshoot the target and with a peak speed between 52 and 68 cm/s. On these trials, the participants received positive feedback (e.g., "great" for peak speeds between 56 and 64 cm/s or "good" for peak speeds between 52 and 56 or 64 and 68 cm/s), and a counter displayed on the screen increased by one point. In contrast, messages of "too fast" or "too slow" were provided when the peak speed exceeded 68 cm/s or did not reach 52 cm/s, respectively. Finally, "overshoot" feedback was provided when the cursor overshot the target (y-axis) by more than 1 cm. Movements were self-paced, as participants were able to take a break before starting the next trial. Short breaks were enforced after approximately 130 trials throughout each session.

Participants were instructed to reach naturally to the target after the go-cue on each trial while the dynamics of the environment were generated by the vBOT. During each movement, the vBOT was either passive (null field), produced a clockwise (CW) or a counterclockwise (CCW) velocity-dependent curl force field, or produced a mechanical channel (error-clamp).

For the velocity-dependent curl field (Gandolfo et al., 1996), the force at the handle was given by:

$$\begin{bmatrix} F_x \\ F_y \end{bmatrix} = \begin{bmatrix} 0 & -1 \\ 1 & 0 \end{bmatrix} \begin{bmatrix} \dot{x} \\ \dot{y} \end{bmatrix}$$

where k was set to either $\pm 10\ \mathrm{N \cdot m^{-1} \cdot s}$, with the sign of k determining the force field direction (CW or CCW). On a channel trial, the reaching movement was confined to a simulated mechanical channel with a stiffness of $6000\ \mathrm{N \cdot m^{-1}}$ and damping of $2\ \mathrm{N \cdot m^{-1} \cdot s}$ acting lateral to the line from the start to the target (Scheidt et al., 2000; Milner and Franklin, 2005). As these trials clamp the lateral error at zero, they are also referred to as error-clamp trials (Smith et al., 2006).

Experimental Paradigm

Participants were required to adapt to an A-B-Error-clamp paradigm (Smith et al., 2006) within dual-adaptation. The A-B-Error-clamp paradigm is a sequential presentation of an adaptation phase (adapting to field A), a de-adaptation phase (presentation of opposing field B), and an error-clamp phase (assessment of any spontaneous recovery). Here the A-B-Error-clamp paradigm was done within dual-adaptation, where participants simultaneously adapt to two opposing force fields. To allow adaptation to two opposing force fields (CW and CCW), two appropriate contextual cues were used. These cues were the workspace visual location (Smith et al., 2006; Howard et al., 2013) either to the left (-10cm from the sagittal axis) or to the right (+10cm from the sagittal axis) of the screen. The physical hand location (proprioceptive location) was the same for both cues, without any shift from the sagittal axis (Figure 1A). Experiments began with a pre-exposure phase where

movements with both contextual cues occured in the null field. Within the adaptation phase one contextual cue (e.g. +10cm visual shift) was associated with one force field (e.g. CW), whereas the other contextual cue (e.g. -10 cm visual shift) was associated with the other force field (e.g. CCW) (Figure 1A,B). In the de-adaptation phase the opposing force fields were then applied to movements for each contextual cue (e.g. CCW for the +10 cm visual shift & CW for the -10cm visual shift) (Figure 1A,B). Finally, error-clamp trials were applied for both contextual cue movements. The experiments were counterbalanced such that in each experiment, half of the participants experienced the adaptation phase with contextual cues matched to one set of force field directions, whereas the other half of the participants had contextual cues matched to the opposing force field directions.

Experiments were built using blocks of trials where each block was composed of 16 trials: 8 with one contextual cue and 8 with the other contextual cue. For most of the experiment, for each contextual cue, seven of the movements were performed in either a null, CW or CCW force field (depending on the experimental phase) while one was performed in the error-clamp. Within a block trials were pseudo randomized.

Experiment 1 (n=10): Ten participants started with 10 blocks in the pre-exposure phase (160 trials). This was followed by 47 blocks in the adaptation phase (752 trials). Within this adaptation phase, after the first 25 blocks, we modified the block structure in order to assess the memory decay for each contextual cue (blocks 26-45). Within these twenty blocks, 5 blocks assessed the decay for one contextual cue (+10 cm visual shift) whereas 5 blocks assessed the decay for the other cue (-10 cm visual shift). These decay blocks alternated between the two contextual cues with a normal block of trials interspersed between them. A

decay block contained an exposure trial of a specific contextual cue followed by a row of 5 error-clamp trials with the same contextual cue. This row of trials was then always followed by an exposure trial of the opposite contextual cue. After these twenty memory decay blocks, two blocks were performed with the original block structure (blocks 46-47). Next, a de-adaptation phase was performed in which the opposite force field was now associated with each contextual cue. The length of the de-adaptation phase was dependent on each participant's performance and could vary between 4 and 25 blocks (64-400 trials). The exact point at which this phase was terminated depended on the difference between the mean of the force compensation measure (see analysis) of the last three error-clamp trials for each contextual cue. These force compensation values were calculated online during the experiment. Once this difference switched sign (became negative) the de-adaptation phase was ended at the end of the current block of trials. Finally participants experienced the error-clamp phase for 20 blocks (320 trials) in which all trials were error-clamps. Within these final blocks, eight error-clamp trials were performed with one contextual cue (+10 cm visual shift) whereas the other eight trials were performed with the other contextual cue (-10 cm visual shift) in a pseudo-randomized order.

Experiment 2 (n=10): The second experiment followed a similar design to the first one, but with specific differences outlined here. After the pre-exposure phase (10 blocks), the adaptation phase lasted for 60 blocks (960 trials). Within the adaptation phase, the memory decay blocks were again applied (blocks 41-50), but with no interspersing normal blocks. Within these memory decays blocks, three error-clamp trials were performed in a row directly after the normal exposure trial for the specific contextual cue. The de-adaptation phase could vary between 4 and 20 blocks (64-320 trials) depending on each participant's performance. In

this experiment, the phase was ended once the mean of the last three force compensation values on the clamp-trials for each cue crossed zero. Finally the error-clamp phase lasted for 10 blocks (160 trials).

Analysis

Data were analyzed offline using MATLAB (2016b, The MathWorks, Natick, MA). Individual trials were aligned on peak velocity, and clipped between -500 ms and +500 ms. All measurements were low-pass filtered at 40 Hz using a 10th order zero-phase-lag Butterworth filter (filtfilt). Over the course of the experiment, the lateral force measured can vary due to the natural drift of the mass of the arm over the airsled. In order to improve our sensitivity of the measurement of the lateral force, we subtracted the mean offset in lateral force for each participant measured before the onset of movement from the total force trace. Specifically the mean force was calculated over all trials for each participant between -250 and -150 ms prior to the movement start. In order to quantify adaptation throughout the experiments, three measures were calculated: kinematic error, force compensation and force profiles.

Kinematic Error. For each non-channel trial (null or curl field trials), the maximum perpendicular error was calculated and used as a measure of kinematic error. The maximum perpendicular error is the signed maximum perpendicular distance between the hand trajectory and the straight line joining the start and end targets.

Force Compensation. On every channel trial (error-clamp trial), the force compensation was calculated to quantify the amount of predictive force adaptation to the force field. Force

compensation is defined on each trial by the regression between the force produced by participants into the wall of the simulated channel (lateral measured force) and the force needed to compensate perfectly for the force field (Smith et al., 2006). The perfect compensatory force can be determined as the forward velocity of each trial multiplied by the force field constant. As experiments were counterbalanced across participants, the values were flipped such that the force compensation associated with each cue has the same sign for every participant. All models used to fit the results of the data assume equal adaptation to both force fields. In order to allow the models to fit the data, we subtracted blockwise the mean force compensation of both contextual cues from the force compensation values for each contextual cue. Therefore the mean compensation across both contextual cues for the whole experiment is zero.

Force Profiles. In order to examine the shape and timing of the predictive forces on channel trials during the experiment, the force profile in the x-axis was normalized by the perfect compensation force profile. This perfect force profile was calculated as the y-axis velocity multiplied by the force field constant.

Throughout the experiments, data are primarily presented for each block. However, a different number of trials (blocks) were performed by each participant in the de-adaptation phase. For plotting purposes, this phase was divided into equal-sized sections, where the mean data was determined for each section rather than for each block in order to allow averaging across participants. For kinematic error twenty sections were used, whereas for force compensation seven sections were used.

Within the adaptation phase of the experiment we had ten decay blocks in which error-clamp trials were repeated several times in a row in order to estimate the memory decay. The memory decay on each trial was calculated as the force compensation on the current error-clamp trial subtracted by the force compensation on the previous error-clamp trial.

Statistics. Using the statistical software JASP (version 0.9.2), repeated measures ANOVAs were run on the kinematic error and the force compensation, with factors *Stage* (4 levels) and *Cue* (2 levels). For comparisons of kinematic error we compared across 4 stages (first 5 blocks in adaptation; final 5 blocks in adaptation; first 5 blocks in de-adaptation; final 5 blocks in de-adaptation). For comparisons of force compensation we compared across a different 4 stages (final 5 blocks in pre-exposure; final 5 blocks in adaptation; final 3 blocks of de-adaptation; all blocks of error-clamp phase). For both ANOVAs the sign of the values for one of the cues was flipped in order to examine whether there were differences in the levels of adaptation between cues. If the main effects were significant ($p<0.05$), post hoc comparisons were performed using the Bonferroni test. In order to examine specific differences in the level of force compensation between the cues, paired t-tests were performed.

Simulations

In order to investigate the computational mechanisms underlying the evolution of dual-adaptation and the formation of motor memories we modeled motor adaptation to two opposing force fields each associated to a contextual cue. For our simulations we examine two models out of a family of learning-from-error equations based on the dual-rate model (Smith et al., 2006):

$$x(n+1) = A \cdot x(n) + B \cdot e(n) \qquad (1)$$

$$e(n) = f(n) - x(n)$$

where:

x(n+1) – output on subsequent trial

x(n) – output on current trial

e(n) – error on current trial

A – retention rate

B – learning rate

f(n) – environmental force

and adaptation occurs through the summation (and competition) of two separate states with different timescales of learning and retention.

In order to model dual-adaptation, we simulate both the "one-fast-two-slow-binary-switch" model (Lee and Schweighofer, 2009):

$$x(n+1) = x_f(n+1) + x_s(n+1) \cdot c(n+1) \qquad (2)$$

$$x_f(n+1) = A_f \cdot x_f(n) + B_f \cdot e(n)$$

$$x_s(n+1) = A_s \cdot x_s(n) + B_s \cdot e(n) \cdot c(n+1)$$

and a "two-fast-two-slow-binary-switch" model:

$$x(n+1) = [x_f(n+1) + x_s(n+1)] \cdot c(n+1) \qquad (3)$$

$$x_f(n+1) = A_f \cdot x_f(n) + B_f \cdot e(n) \cdot c(n+1)$$

$$x_s(n+1) = A_s \cdot x_s(n) + B_s \cdot e(n) \cdot c(n+1)$$

on a A-B-Error-clamp paradigm similar to our experiment. For our simulations, the parameters were arbitrarily set at A_f=0.92 and B_f=0.05 for the fast process and A_s=0.999 and B_s=0.01 for the slow process.

Model Fitting

The experimental data was fit by twelve models from a family of learning-from-error equations (Equation 1). In a previous study (Lee and Schweighofer, 2009) assumed the contextual switch (c) between the cues was binary. However, other models of sensorimotor learning such as the MOSAIC model (Kawato, 1999; Haruno et al., 2001), have suggested a responsibility estimator that would provide a weighted mixture between modules. In order to examine both of these possibilities, we set the contextual switch as binary for half of the models and as a parameter (c) for the other half of the models.

Specifically, we fit twelve models with parallel organization between the fast and slow processes. These consisted of a dual-rate, a triple-rate and a quadruple-rate model where each could be built with either one fast process or multiple fast processes and where the contextual cue switch was either binary or weighted. The general equation of these models can be written:

$$x(n+1) = x_f(n+1) + [x_s(n+1) + x_{us}(n+1) + x_{hs}(n+1)]\cdot c(n+1) \quad (4)$$

for models containing a single fast process or

$$x(n+1) = [x_f(n+1) + x_s(n+1) + x_{us}(n+1) + x_{hs}(n+1)]\cdot c(n+1) \quad (5)$$

for models containing multiple fast processes.

Therefore, the fast process contains either a single state and is written as

$$x_f(n+1) = A_f\cdot x_f(n) + B_f\cdot e(n) \quad (6)$$

or multiple states and is written as

$$x_f(n+1) = A_f\cdot x_f(n) + B_f\cdot e(n)\cdot c(n+1) \quad (7)$$

The slow, "ultraslow" and "hyperslow" processes (Inoue et al., 2010) contain multiple states and are written:

$$x_s(n+1) = A_s\cdot x_s(n) + B_s\cdot e(n)\cdot c(n+1) \quad (8)$$

$$x_{us}(n+1) = A_{us}\cdot x_{us}(n) + B_{us}\cdot e(n)\cdot c(n+1) \quad (9)$$

$$x_{hs}(n+1) = A_{hs}\cdot x_{hs}(n) + B_{hs}\cdot e(n)\cdot c(n+1) \quad (10)$$

with

$x_{us}(n) = 0$ for the dual-rate models,

$x_{hs}(n) = 0$ for the dual-rate and triple-rate models.

Here the hyperslow process has a lower learning rate and higher retention rate than the ultraslow process. The one-fast-two-slow-binary-switch model (Lee and Schweighofer, 2009) was used as our referent model (eq. 2).

Each model was fit to the force compensation data throughout an entire experiment. In order to fit the models, the mean force compensation values over the two cues was subtracted to remove any potential bias between the cues. For each model, we found the parameter values that best fit the experimental data, using a least-squares method (fminsearchbnd), where the parameters were constrained:

$0.5<A_f<0.95<A_s,A_{us},A_{hs}<1$;

$0<B_{hs}<B_{us}<B_s<0.1<B_f<0.3$;

The parameters were simultaneously fit to each participant's data within each of the two experiments initially. In order to examine model fits across both experiments, the parameters were then fit to each participant's data for both experiments simultaneously.

In order to compare across the models, Bayesian information criterion (BIC) was calculated and used to select the preferred model (lowest BIC). If the difference between two BIC values is between 0 to 2 there is considered to be no difference between the models, between 2 to 6 the difference is considered to be positive (small but existing), between 6 to 10 the difference is considered to be strong, and a difference exceeding 10 is described as very strong (Kass and Raftery, 1995). Specifically we calculated the improvement in BIC value, defined as the difference between the BIC value of the referent model and the other models. A BIC improvement of greater than 4.6 therefore indicates a strong improvement compared to the one-fast-two-slow-binary-switch model.

Results

Here we assess the formation and the recall of motor memories while simultaneously learning two opposing force fields. Previous research (Lee and Schweighofer, 2009) proposed that the one-fast-two-slow-state model of motor adaptation best fit the data of dual-adaptation. Here we simulate both the one-fast-two-slow-state model and the two-fast-two-slow-state model of motor adaptation in order to determine whether these two models have specific differences in their predictions of the classic adaptation-de-adaptation-error-clamp experiment (Smith et al., 2006). Specifically here we simulate these two models of motor adaptation for a dual-adaptation task in which each task was associated with a cue, similar to our experimental design. These learning models update the motor state on the next trial as a function of the current motor state and the error experienced on that trial (Smith et al., 2006). In the simulation, the number of trials of the de-adaptation phase were adjusted such that the adaptation phase ended when the total motor state output returned to zero for the one-fast-two-slow-state model. The same number of trials was used for the other model.

The simulation of the two models predicts different motor outputs during the error-clamp phase (Figure 2). In the one-fast-two-slow model (Figure 2A), the single fast process (dashed purple line) is continually updating to both opposing force fields and therefore learns an output close to zero (mean of both force fields). The total output (thick red and blue lines) are therefore almost entirely driven by the two slow processes (dotted lines). In this case, de-adaptation, where the total output is driven towards zero, requires the active unlearning of the two slow processes, erasing the motor memories of the previously learned tasks. Finally in the error-clamp phase the total output remains at zero as both the slow and

fast processes have outputs close to zero. In contrast, the two-fast-two-slow model (Figure 2B) has separate slow and fast processes for each contextual cue (and therefore force field). In this case, the total motor output for each cue (red or blue thick lines) exhibits a similar pattern to that seen for a single adaptation task (Smith et al., 2006). In particular, adaptation to each force field occurs through the update of the respective slow and fast processes gated by the contextual cue. The total motor output in early adaptation is mostly due to the fast process (dashed line) whereas in late adaptation the slow process (dotted lines) contributes most. De-adaptation occurs primarily through updates of the fast process, such that the total motor output returns to zero. However at this stage the slow process still retains most of the learned motor memory. Finally in the error-clamp phase both the slow and fast processes gradually decay to zero but at different rates. In contrast to the previous model, the slow process still retains much of the learned memory, resulting in a rebound of the total output towards the first learned task - a process called spontaneous recovery. Therefore these two models make very specific testable predictions. If the one-fast two-slow model is correct, we will see no spontaneous recovery in a dual-task paradigm. Conversely, if the two-fast-two-slow model is correct, we will find evidence of spontaneous recovery. In order to test the predictions of our two models, two experiments were conducted in which a total of twenty participants performed a dual-adaptation task.

Experiment 1

Experimental Results. Ten participants performed forward reaching movements in the same physical location while two contextual cues were provided (visual feedback of the movement in the left or right half of the workspace, Figure 1B). We investigated differences in the

kinematic error throughout the experiment using a repeated measures ANOVA with main effects of stage (4 levels: early exposure, late exposure, early de-adaptation and late de-adaptation) and cue (2 levels). We found a significant main effect of stage ($F_{3,27}$=48.672; $p<0.001$) and of cue ($F_{1,9}$=5.607; p=0.042). A similar repeated measures ANOVA was performed on the force compensation resulting in a significant main effect of stage ($F_{3,27}$=281.688; $p<0.001$) but no significant effect of cue ($F_{1,9}$=0.004; p=0.954). Further differences between specific stages in the experiment were then examined using post-hoc comparisons below.

In the pre-exposure phase, the movements were close to a straight trajectory with kinematic error (Figure 3A) and force compensation (Figure 3B) remaining close to zero. There was no difference in the force compensation between the two cues over the last 5 blocks (paired t-test: t_9=0.743; p=0.476) and the force profiles for the two contextual cues were not distinguishable (Figure 3C).

In the adaptation phase, each contextual cue was associated with one of two curl force fields (clockwise and counterclockwise). As expected, initial trials in this adaptation phase exhibited large kinematic errors in the lateral directions, as the force field associated to each cue perturbed the movements in opposite directions (Figure 3A, red and blue curves). Throughout the adaptation phase participants gradually reduced their kinematic error from initial to final adaptation, (post-hoc comparison: $p<0.001$) across both cues (Figure 3A). During this same phase, the force compensation (Figure 3B) increased gradually until it plateaued near 80% of perfect force compensation to each force field. A post hoc comparison showed an increase in force compensation between pre-exposure and final adaptation phases ($p<0.001$). The force

profiles at the end of adaptation (last 10 blocks) demonstrate a bell-shaped profile similar to their forward velocity throughout the movement (Figure 3D). This pattern indicates a predictive compensation for both of the velocity-dependent curl force-fields. This result, combined with the reduction in kinematic error, demonstrates that participants were able to adapt to the two opposing force fields simultaneously, supporting the finding that visual workspace location is a strong contextual cue for dual-adaptation (Howard et al., 2013).

In the following de-adaptation phase, the association between the force fields and contextual cues were flipped in order to reduce the total output of predictive compensation to zero. The initial trials in this phase show a large kinematic error in the opposite direction to that in the initial exposure trials (Figure 3A). Over the following blocks in the de-adaptation phase the kinematic error was reduced until it was similar in size (but opposite in direction) to the initial adaptation trials (post hoc comparison, $p=0.249$). The force compensation (Figure 3B) rapidly decreases in this phase until there are no significant differences between the force compensation for the two contextual cues (paired t-test: $t_9=0.409$; $p=0.692$). This is further supported by the force profiles at the end of the de-adaptation phase (Figure 3E), which shows similar forces for each of the two contextual cues. Therefore at the end of the de-adaptation phase there were no differences in the total predictive force output for the two contextual cues.

Finally, in the error-clamp phase, channel trials clamp the lateral error to zero in order to assess the presence of any spontaneous recovery -- rebound of the predictive force towards the initial adaptation. Force compensation shows a quick rebound towards the initial adaptation (Figure 3B) (post hoc comparison versus last 3 blocks in de-adaptation phase: $p=0.016$)

438 followed by a negligible decay of the motor output throughout the twenty blocks. This
439 evidence for spontaneous recovery is supported by the significant difference between the
440 force compensation for the two contextual cues (paired t-test: t_9=-6.538; p<0.001) across all
441 twenty blocks. The force profiles during this error-clamp phase show predictive forces in the
442 appropriate direction for compensation to the initial learned force field (Figure 3F). These
443 force profiles peak near the time of peak velocity, but are reduced in size compared to those in
444 the adaptation phase (Figure 3D). Together these results demonstrate that the participants
445 maintain part of the memory of the initially learned task - arguing against the idea that
446 dual-adaptation can be modelled by a one-fast two-slow-state model.

447 Model Fitting. Models from a family of learning-from-error equations were fitted to the
448 participants' force compensation data and compared using Bayesian Information Criterion
449 (BIC). While Lee and Schweighofer (Lee and Schweighofer, 2009) found that a
450 one-fast-two-slow model best fit their experimental data, any evidence for spontaneous
451 recovery argues against this model (Figure 2). Our experimental results therefore suggest that
452 the two-fast-two-slow state model better explains dual-adaptation. If we compare the BIC
453 between these two models, the two-fast-two-slow model exhibits a BIC improvement of 2626,
454 strongly suggesting the existence of two fast processes. However, other models of
455 dual-adaptation might also be consistent with our results. Therefore, to further investigate
456 motor memory formation, we expanded our range of models to include both additional states
457 (ultraslow and hyperslow) and a weighted gating of the contextual cues, producing a total of
458 twelve models. In this experiment (Figure 4), two models, the
459 two-fast-weighted-switch-triple-rate model and the one-fast-binary-switch-quadruple-rate

model, perform better than the other models (BIC improvement > 6). However, no significant difference is found between the two best models, (BIC difference = 0.25).

Experiment 2

Experimental results. Ten participants performed experiment 2. The major difference between this and experiment 1 was the criterion for ending the de-adaptation phase and proceeding to the error-clamp phase (Figure 1B). Participants performed 240±26 trials in the de-adaptation phase compared to 211±30 trials in experiment 1. Overall the pattern of the experimental results was similar to the first study. There were significant main effects of stage ($F_{3,27}$=59.595; p<0.001) but not cue ($F_{1,9}$=0.053; p=0.824) for the kinematic error across the whole experiment. Similarly force compensation showed a main effect of stage ($F_{3,27}$=341.561; p<0.001) but not cue ($F_{1,9}$=0.002; p=0.966). Initial movements in the pre-exposure phase exhibited little kinematic error (Figure 5A) and no difference between the two cues in force compensation (paired t-test: t_9=0.429; p=0.678) over the 5 last blocks (Figure 5B) or force profiles (Figure 5C).

Initial trials in the adaptation phase exhibited large lateral kinematic errors. These kinematic errors gradually reduced from initial to final adaptation (post hoc comparisons: p<0.001). During this same phase, the force compensation (Figure 5B) increased gradually, plateauing around 80%. A post hoc comparison showed an increase in force compensation between pre-exposure and final adaptation phases (post hoc comparisons: p<0.001). The force profiles at the end of adaptation exhibit a bell-shaped profile (Figure 5D) indicating predictive compensation for both of the velocity-dependent curl force-fields.

In the de-adaptation phase, the initial trials show a large kinematic error in the opposite direction to that in the initial exposure trials (Figure 5A). This error reduced until it was similar in size (but opposite direction) to the initial adaptation trials (post hoc comparisons: $p=1.000$). Here, de-adaptation required participants to deadapt independently to both cues resulting in a further de-adaptation compared to experiment 1. In fact, we observe force profiles which are already adapting to the opposing force field (Figure 5E), and find a significant difference in the force compensation between the two cues (paired t-test: $t_9=4.479$; $p=0.002$).

In the error-clamp phase, the force compensation exhibits a quick rebound towards the initial adaptation (Figure 5B) (post hoc comparison versus last 3 blocks in de-adaptation phase: $p<0.001$) which is maintained over the rest of the phase. This evidence for spontaneous recovery is again supported by the significant difference between the force compensation for the two contextual cues (paired t-test for all blocks : $t_9=-4.400$; $p=0.002$). The force profiles show predictive forces in the appropriate direction for compensation to the initial learned force field (Figure 5F). Again, the results of experiment 2 argue against the one-fast-two-slow-state model by demonstrating spontaneous recovery.

Model fitting.

The twelve multi-rate models were fit to the data of experiment 2 and compared using BIC (Figure 6). Here the two-fast-triple-rate model with binary switching provided a better fit than all the other models (BIC improvement > 10) with the exception of the

two-fast-triple-rate model with weighted switching (BIC improvement > 6). Interestingly, all two-fast models (weighted or binary) performed better (higher BIC improvement) than the one-fast models within each set of models with the same number of rates (e.g. within the quadruple-rate models).

Combined Model Fitting

Finally, to determine which model or models best fit the two independent experiments, we fit all twelve multi-rate models to the experimental data of both experiments simultaneously (Figure 7). Here the best-fit model is the two-fast-triple-rate-binary-switch model (BIC improvement > 6). The weighted switch version of the same model was the only model within a BIC of 10 compared to this best-fit model. Together the results demonstrate strong support for two fast processes and the existence of a third timescale - an "ultraslow" rate - that has a slower learning rate and a higher retention rate than the "slow" process. In addition, the parameters of these two best fit models (Table 1) are similar suggesting that the difference between these two models is small. The weighted contextual switch (parameter c) has a value of 0.92 compared to the value of 1.0 for the binary-switch model. As these parameters are similar under the conditions of our experiment, the BIC penalizes this model for its additional parameter. Therefore, for the contextual cues studied in this experiment (e.g. visual location), the evidence argues in favor of binary switching.

Discussion

Here we investigated the structure of motor memory formation during force field adaptation. Specifically we tested the existence of one or multiple fast processes during adaptation by applying the A-B-Error-clamp paradigm (Smith et al., 2006) within dual-adaptation (Howard et al., 2013). Participants initially adapted to two opposing force fields each associated with distinct contextual cues. After adaptation, the association between the contextual cues and the force fields were reversed, driving de-adaptation of the predictive force towards zero. Finally the kinematic error was clamped at zero to assess the presence or absence of spontaneous recovery. In two experiments we found evidence for spontaneous recovery, supporting the two-fast-dual-rate model over the single-fast-dual-rate model. However, by comparing the fits of twelve models over a range of timescales, we found that a two-fast-triple-rate model with binary switching best explained the experimental results. These results argue against previous models suggesting only a single fast process (Lee and Schweighofer, 2009) and support the existence of longer timescales in motor adaptation.

The combination of both fast and slow processes have been suggested to be necessary to account for spontaneous recovery (Smith et al., 2006; Criscimagna-Hemminger and Shadmehr, 2008; Ethier et al., 2008; Lee and Schweighofer, 2009; Coltman et al., 2019). Our results, exhibiting spontaneous recovery of the initially learned force field for each contextual cue, support the existence of both two slow and two fast processes in motor adaptation. However, while simulations of the dual-rate model show that multiple fast processes are

required to exhibit spontaneous recovery, the only requirement is multiple timescales for each contextual cue. That is, spontaneous recovery could also occur through the combination of the slow process with an even slower one (e.g. ultraslow process). In any case, during the error-clamp phase the remaining slower memory is revealed as the faster process decays to zero. Therefore, in order to examine whether or not there are multiple fast processes, we fit the data with a variety of models using BIC for model comparison. Across both experiments, the two best fitting models were a triple-rate with two fast processes, providing further evidence that there are independent fast processes for each motor memory and arguing against previous findings (Lee and Schweighofer, 2009).

The two best-fit models (triple-rate with two fast processes) differ only in the contextual cue switch that gates the two motor memories. While the model with binary switching was preferred over the model with weighted cue switching, we suggest that this depends on the specific contextual cue used. That is, separation of the movements in visual space, as examined in our study, is an extremely strong contextual cue for the learning of multiple dynamics (Hirashima and Nozaki, 2012; Howard et al., 2013) suggesting a weighting close to one as seen in our results (c=0.92). Other cues, such as background color, object orientation (Howard et al., 2013), or static visual cues (Howard et al., 2012) which do not allow the formation of separate motor memories, might have weights closer to 0.5. Indeed, several force field generalization studies (Sarwary et al., 2015; Howard et al., 2017; Sadeghi et al., 2018) have shown that contextual cues do not serve as discrete switches but instead weight the contributions of associated motor memories. This matches the concept of multiple paired models for sensorimotor control (Wolpert and Kawato, 1998). In these models, each internal model or motor memory is selected by a responsibility predictor that determines its

contribution to the overall motor output based on contextual information (Kawato, 1999; Haruno et al., 2003). We suggest that our results argue for a similar framework where the selection of each motor memory is based on a weighted input where the weight depends on the likelihood that this contextual cue predicts the next task.

Many previous studies have supported the dual-rate model to explain adaptation (Smith et al., 2006; Criscimagna-Hemminger and Shadmehr, 2008; Ethier et al., 2008; Lee and Schweighofer, 2009; Coltman et al., 2019). However these studies have primarily focussed only on short-term adaptation, examining at most several hundred movements. Consequently, in such short experiments an architecture consisting of two timescales may be sufficient to explain adaptation to a new task. Nevertheless, in daily life, we are often exposed to tasks or changes in environment over days or years. Indeed it commonly requires many months or years of practice to master a motor skill (e.g. using chopsticks or skiing). Once these skills are learned, people are able to recall them perfectly. In these cases, it is clear that a model of adaptation with only two timescales is insufficient to explain the formation of motor memories. Recent computational and behavioral studies have suggested the existence of longer timescales (Robinson et al., 2006; Kording et al., 2007; Inoue et al., 2010) such as an ultraslow process in motor adaptation, which are further supported by our results.

Both our study and that of (Inoue et al., 2010) support the existence of longer timescales in adaptation and have shown little decay during the error-clamp phase after more extensive training phases. Our results, found with a design where participants initially adapted to a force field for over 750 trials, suggests a triple-rate model of adaptation. However, we expect that for studies with longer training periods, the number of active timescales would

increase. That is, we propose that there is a continuum of timescales in human motor learning, where the active number of timescales used for any given task depends on the overall time over which such a task is practiced (minutes, hours, days, or years) and the relative relevance of such learning for the future (Berniker and Kording, 2008, 2011; Wei and Körding, 2009; Wei and Kording, 2018). These longer timescales, with slow learning rates and almost no decay, act to protect the motor memories and could explain why we never forget some tasks, such as riding a bicycle.

One major question is where such learning timescales might be implemented within the sensorimotor system. While many studies have suggested that the cerebellum is necessary for initial adaptation (Smith and Shadmehr, 2005; Galea et al., 2011), recent papers have suggested the primary motor cortex (M1) for the storage of these motor memories (Tanaka et al., 2009; Galea et al., 2011). That is, there could be a shift from the cerebellum to M1, or that the fast process occurs within the cerebellum while the slow process occurs within M1. Further support has come from the finding that cerebellar patients adapt better to slow rather than abrupt changes in dynamics, suggesting the involvement of the cerebellum in the fast adaptation processes (Tseng et al., 2007; Criscimagna-Hemminger et al., 2010). However, support for longer timescales in motor adaptation has also been brought from neuroimaging studies. Specifically, different brain networks have been shown to be activated in at least three different timescales in dual-adaptation (Kim et al., 2015) with distinct regions of the cerebellum involved in both the fast and slow timescales. Thus, perhaps learning on multiple timescales takes place across multiple regions rather than shifting from one region to another.

The cerebellum has been implicated in storing multiple internal models (Imamizu et al., 2003, 2004; Kim et al., 2015). Indeed, fMRI decoding has shown separate representations for different visuomotor mappings, with distinct substrates for each rotation in both the supplementary motor area and cerebellum (Ogawa and Imamizu, 2013). However, none of these studies have been able to establish the existence of distinct representations for the fast timescale. Our results predict distinct representations due to the multiple fast processes, but the degree to which these might be spatially separable is unknown. Recent work has shown that rapid force field adaptation does not require changes in connectivity (Perich et al., 2018) or neural tuning (Perich and Miller, 2017), but instead may result from changes output-null subspace between the premotor (PMd) and M1 areas in order to produce rapid adaptation to the changed dynamics (Perich et al., 2018). In this case, distinct spatial representations of multiple fast processes may not be possible to detect with current neuroimaging techniques.

Overall, here we expand the concept of the dual-rate model (Smith et al., 2006) into the framework of multiple paired models for sensorimotor control (MOSAIC model; (Wolpert and Kawato, 1998). Originally, the architecture of the MOSAIC model allows the learning of multiple paired inverse and forward models, by selecting the appropriate module (or modules) for the current environment. Built from Bayesian theories, this model uses a responsibility predictor to switch between (or combine) relevant modules based on contextual information (Kawato, 1999; Haruno et al., 2003). We extend this framework by suggesting that these paired models are formed through adaptation on multiple timescales (e.g. fast, slow and ultraslow processes) (Figure 8). Whether or not the inverse and forward models are represented on different timescales (Flanagan et al., 2003) is not yet established. However, our

results demonstrate both the existence of independent fast processes for each motor module and the presence of longer timescales in motor adaptation.

References

Berniker M, Kording K (2008) Estimating the sources of motor errors for adaptation and generalization. Nat Neurosci 11:1454–1461.

Berniker M, Kording KP (2011) Estimating the relevance of world disturbances to explain savings, interference and long-term motor adaptation effects. PLoS Comput Biol 7:e1002210.

Brashers-Krug T, Shadmehr R, Bizzi E (1996) Consolidation in human motor memory. Nature 382:252–255.

Caithness G, Osu R, Bays P, Chase H, Klassen J, Kawato M, Wolpert DM, Flanagan JR (2004) Failure to consolidate the consolidation theory of learning for sensorimotor adaptation tasks. J Neurosci 24:8662–8671.

Coltman SK, Cashaback JGA, Gribble PL (2019) Both fast and slow learning processes contribute to savings following sensorimotor adaptation. J Neurophysiol 121:1575–1583.

Conditt MA, Gandolfo F, Mussa-Ivaldi FA (1997) The motor system does not learn the dynamics of the arm by rote memorization of past experience. J Neurophysiol 78:554–560.

Criscimagna-Hemminger SE, Bastian AJ, Shadmehr R (2010) Size of error affects cerebellar contributions to motor learning. J Neurophysiol 103:2275–2284.

Criscimagna-Hemminger SE, Shadmehr R (2008) Consolidation patterns of human motor memory. J Neurosci 28:9610–9618.

Ethier V, Zee DS, Shadmehr R (2008) Spontaneous recovery of motor memory during saccade adaptation. J Neurophysiol 99:2577–2583.

Flanagan JR, Vetter P, Johansson RS, Wolpert DM (2003) Prediction precedes control in motor learning. Curr Biol 13:146–150.

Franklin DW, Burdet E, Tee KP, Osu R, Chew C-M, Milner TE, Kawato M (2008) CNS learns stable, accurate, and efficient movements using a simple algorithm. J Neurosci 28:11165–11173.

Galea JM, Vazquez A, Pasricha N, de Xivry J-JO, Celnik P (2011) Dissociating the roles of the cerebellum and motor cortex during adaptive learning: the motor cortex retains what the cerebellum learns. Cereb Cortex 21:1761–1770.

Gandolfo F, Mussa-Ivaldi FA, Bizzi E (1996) Motor learning by field approximation. Proceedings of the National Academy of Sciences 93:3843–3846 Available at: http://dx.doi.org/10.1073/pnas.93.9.3843.

Haruno M, Wolpert DM, Kawato M (2001) Mosaic model for sensorimotor learning and control.

Neural Comput 13:2201–2220.

Haruno M, Wolpert DM, Kawato M (2003) Hierarchical MOSAIC for movement generation. International Congress Series 1250:575–590 Available at: http://dx.doi.org/10.1016/s0531-5131(03)00190-0.

Herzfeld DJ, Vaswani PA, Marko MK, Shadmehr R (2014) A memory of errors in sensorimotor learning. Science 345:1349–1353.

Hirashima M, Nozaki D (2012) Distinct motor plans form and retrieve distinct motor memories for physically identical movements. Curr Biol 22:432–436.

Howard IS, Ford C, Cangelosi A, Franklin DW (2017) Active lead-in variability affects motor memory formation and slows motor learning. Sci Rep 7:7806.

Howard IS, Ingram JN, Franklin DW, Wolpert DM (2012) Gone in 0.6 seconds: the encoding of motor memories depends on recent sensorimotor states. J Neurosci 32:12756–12768.

Howard IS, Ingram JN, Wolpert DM (2009) A modular planar robotic manipulandum with end-point torque control. J Neurosci Methods 181:199–211.

Howard IS, Wolpert DM, Franklin DW (2013) The effect of contextual cues on the encoding of motor memories. Journal of Neurophysiology 109:2632–2644 Available at: http://dx.doi.org/10.1152/jn.00773.2012.

Imamizu H, Kuroda T, Miyauchi S, Yoshioka T, Kawato M (2003) Modular organization of internal models of tools in the human cerebellum. Proc Natl Acad Sci U S A 100:5461–5466.

Imamizu H, Kuroda T, Yoshioka T, Kawato M (2004) Functional magnetic resonance imaging examination of two modular architectures for switching multiple internal models. J Neurosci 24:1173–1181.

Inoue M, Uchimura M, Karibe A, Kitazawa S (2010) Three different timescales in prism adaptation. Neuroscience Research 68:e278 Available at: http://dx.doi.org/10.1016/j.neures.2010.07.1236.

Izawa J, Shadmehr R (2011) Learning from sensory and reward prediction errors during motor adaptation. PLoS Comput Biol 7:e1002012.

Karniel A, Mussa-Ivaldi FA (2002) Does the motor control system use multiple models and context switching to cope with a variable environment? Exp Brain Res 143:520–524.

Kass RE, Raftery AE (1995) Bayes Factors. Journal of the American Statistical Association 90:773 Available at: http://dx.doi.org/10.2307/2291091.

Kawato M (1999) Internal models for motor control and trajectory planning. Curr Opin Neurobiol 9:718–727.

Kim S, Ogawa K, Lv J, Schweighofer N, Imamizu H (2015) Neural Substrates Related to Motor Memory with Multiple Timescales in Sensorimotor Adaptation. PLoS Biol 13:e1002312.

Kojima Y, Iwamoto Y, Yoshida K (2004) Memory of learning facilitates saccadic adaptation in the monkey. J Neurosci 24:7531–7539.

Kording KP, Tenenbaum JB, Shadmehr R (2007) The dynamics of memory as a consequence of

optimal adaptation to a changing body. Nat Neurosci 10:779–786.

Krakauer JW, Ghez C, Ghilardi MF (2005) Adaptation to visuomotor transformations: consolidation, interference, and forgetting. J Neurosci 25:473–478.

Krakauer JW, Ghilardi MF, Ghez C (1999) Independent learning of internal models for kinematic and dynamic control of reaching. Nat Neurosci 2:1026–1031.

Lee J-Y, Schweighofer N (2009) Dual adaptation supports a parallel architecture of motor memory. J Neurosci 29:10396–10404.

Medina JF, Garcia KS, Mauk MD (2001) A mechanism for savings in the cerebellum. J Neurosci 21:4081–4089.

Milner TE, Franklin DW (2005) Impedance control and internal model use during the initial stage of adaptation to novel dynamics in humans. J Physiol 567:651–664.

Nozaki D, Kurtzer I, Scott SH (2006) Limited transfer of learning between unimanual and bimanual skills within the same limb. Nat Neurosci 9:1364–1366.

Ogawa K, Imamizu H (2013) Human sensorimotor cortex represents conflicting visuomotor mappings. J Neurosci 33:6412–6422.

Oldfield RC (1971) The assessment and analysis of handedness: the Edinburgh inventory. Neuropsychologia 9:97–113.

Osu R, Hirai S, Yoshioka T, Kawato M (2004) Random presentation enables subjects to adapt to two opposing forces on the hand. Nat Neurosci 7:111–112.

Perich MG, Gallego JA, Miller LE (2018) A Neural Population Mechanism for Rapid Learning. Neuron 100:964–976.e7.

Perich MG, Miller LE (2017) Altered tuning in primary motor cortex does not account for behavioral adaptation during force field learning. Experimental Brain Research 235:2689–2704 Available at: http://dx.doi.org/10.1007/s00221-017-4997-1.

Robinson FR, Soetedjo R, Noto C (2006) Distinct short-term and long-term adaptation to reduce saccade size in monkey. J Neurophysiol 96:1030–1041.

Sadeghi M, Ingram JN, Wolpert DM (2018) Adaptive coupling influences generalization of sensorimotor learning. PLoS One 13:e0207482.

Sarwary AME, Stegeman DF, Selen LPJ, Medendorp WP (2015) Generalization and transfer of contextual cues in motor learning. J Neurophysiol 114:1565–1576.

Scheidt RA, Reinkensmeyer DJ, Conditt MA, Rymer WZ, Mussa-Ivaldi FA (2000) Persistence of motor adaptation during constrained, multi-joint, arm movements. J Neurophysiol 84:853–862.

Smith CD, Walton A, Loveland AD, Umberger GH, Kryscio RJ, Gash DM (2005) Memories that last in old age: motor skill learning and memory preservation. Neurobiol Aging 26:883–890.

Smith MA, Ghazizadeh A, Shadmehr R (2006) Interacting adaptive processes with different timescales underlie short-term motor learning. PLoS Biol 4:e179.

Smith MA, Shadmehr R (2005) Intact Ability to Learn Internal Models of Arm Dynamics in

Huntington's Disease But Not Cerebellar Degeneration. Journal of Neurophysiology 93:2809–2821 Available at: http://dx.doi.org/10.1152/jn.00943.2004.

Tanaka H, Sejnowski TJ, Krakauer JW (2009) Adaptation to visuomotor rotation through interaction between posterior parietal and motor cortical areas. J Neurophysiol 102:2921–2932.

Trent MC, Ahmed AA (2013) Learning from the value of your mistakes: evidence for a risk-sensitive process in movement adaptation. Front Comput Neurosci 7:118.

Tseng Y-W, Diedrichsen J, Krakauer JW, Shadmehr R, Bastian AJ (2007) Sensory prediction errors drive cerebellum-dependent adaptation of reaching. J Neurophysiol 98:54–62.

Wei K, Körding K (2009) Relevance of error: what drives motor adaptation? J Neurophysiol 101:655–664.

Wei K, Kording KP (2018) Behavioral tracking gets real. Nature Neuroscience 21:1146–1147 Available at: http://dx.doi.org/10.1038/s41593-018-0215-0.

Wolpert DM, Kawato M (1998) Multiple paired forward and inverse models for motor control. Neural Netw 11:1317–1329.

Wolpert DM, Miall RC, Kawato M (1998) Internal models in the cerebellum. Trends Cogn Sci 2:338–347.

Figures

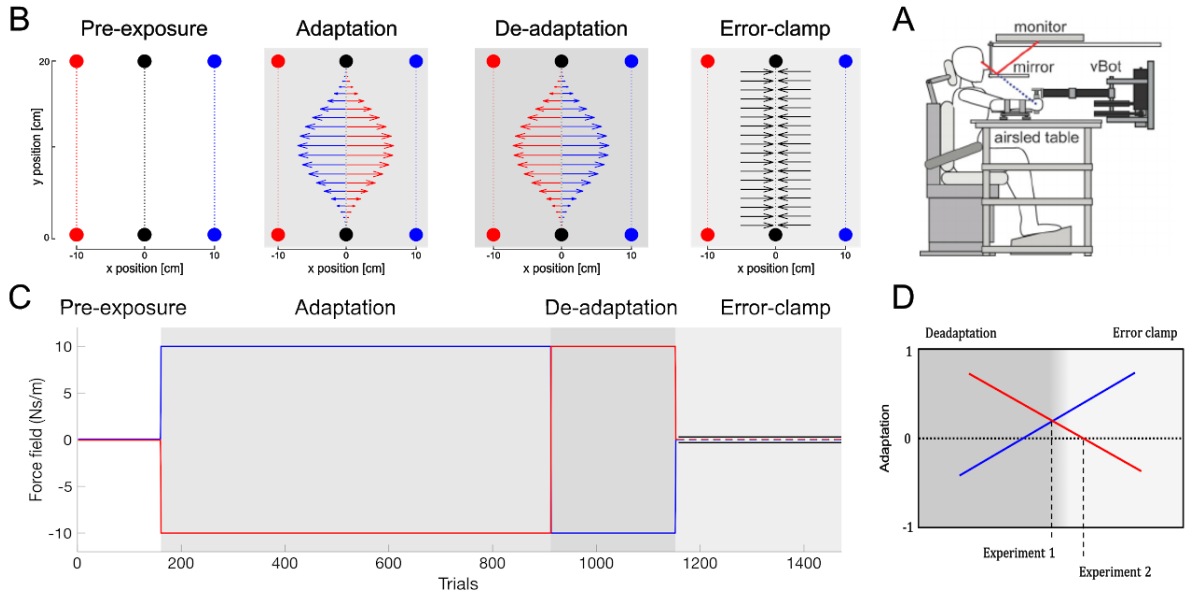

Figure 1. Experimental Setup and Paradigm. **A.** Participants were seated and grasped the handle of the robotic manipulandum (vBOT) with their forearm supported by an airsled. Visual feedback of movements, displayed by the monitor, were viewed through a mirror so that they appear in the plane of movement. **B.** Workspace layout of the experiment. Participants always physically performed forward reaching movements in the center of the workspace (black). During these physical movements, the visual feedback (targets and cursor) was presented at one of two visual workspaces (red and blue) which acted as a contextual cue: -10cm offset (left workspace) set as cue 1 and +10cm offset (right workspace) set as cue 2. Red and blue colors are only used for illustration. On any one trial, only one of the visual workspaces was presented. In each phase of the experiment, different force fields were generated. In the pre-exposure phase, no external force was applied on the handle by the robot (null field trials). In the adaptation phase, two force fields were applied (CW and CCW), where each force field was always associated with one of the contextual cues (e.g. CCW force field for the left visual workspace and CW force field for the right visual workspace. In the de-adaptation phase, the association of the force fields to the visual cues was reversed (e.g. CW force field for the left visual workspace and CCW force field for the right visual workspace. In the error-clamp phase, all movements were performed in mechanical channel for both contextual cues. **C.** Temporal structure of the experiment. The different force field parameters depend on the experimental phase in order to create an A-B-error-clamp paradigm. In the error-clamp phase (light grey), the kinematic error is held at zero to assess spontaneous recovery. Trial numbers are shown for experiment 1. **D.** The participant-dependent transition from the de-adaptation to the error-clamp phase differed between the two experiments. In experiment 1, the participant's predictive adaptation (force compensation) for the two cues had to cross one another. In experiment 2, the participant's predictive adaptation was required to change sign (cross zero-line) for both cues.

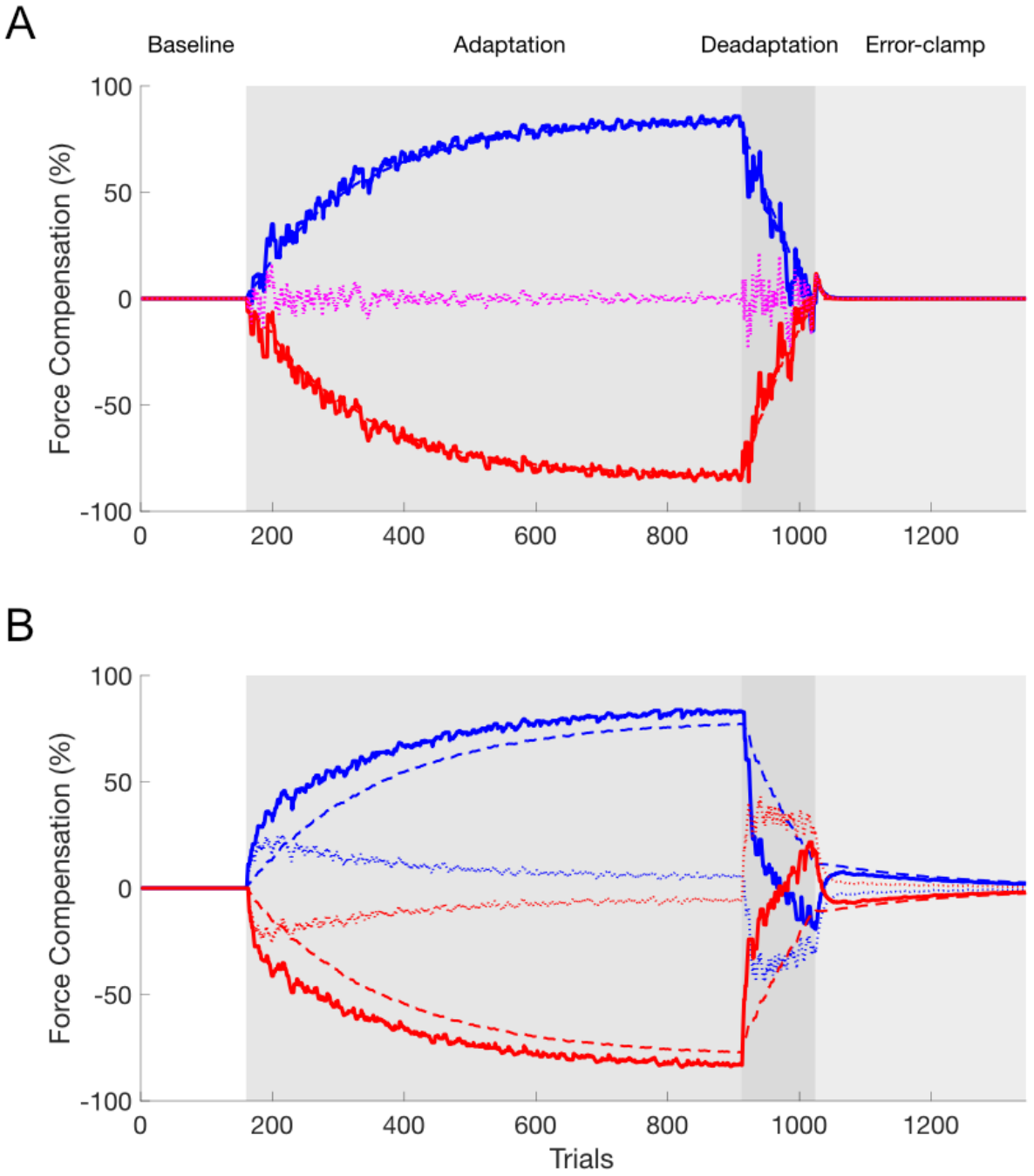

Figure 2. Simulation of the the dual-rate model in dual-adaptation to compare a structure with one fast process (**A**) against a structure with two fast processes (**B**). The model output of the contextual cue 1 (left workspace shift) and 2 (right workspace shift) are presented with red and blue lines, respectively. **A.** The dual-rate model of motor adaptation with one fast process and two slow processes. The total output for each contextual cue (red and blue thick lines) is composed of the summation of each slow process (red and blue dashed lines) and the single fast process (magenta dotted line). Note the absence of any spontaneous recovery. **B.** The dual-rate model of motor adaptation with two fast and two slow processes. The total output for each contextual cue (red and blue thick lines) is composed of the summation of each fast (red and blue dotted lines) and slow (red and blue dashed lines) process. Note that spontaneous recovery is revealed for both contextual cues in the error-clamp phase.

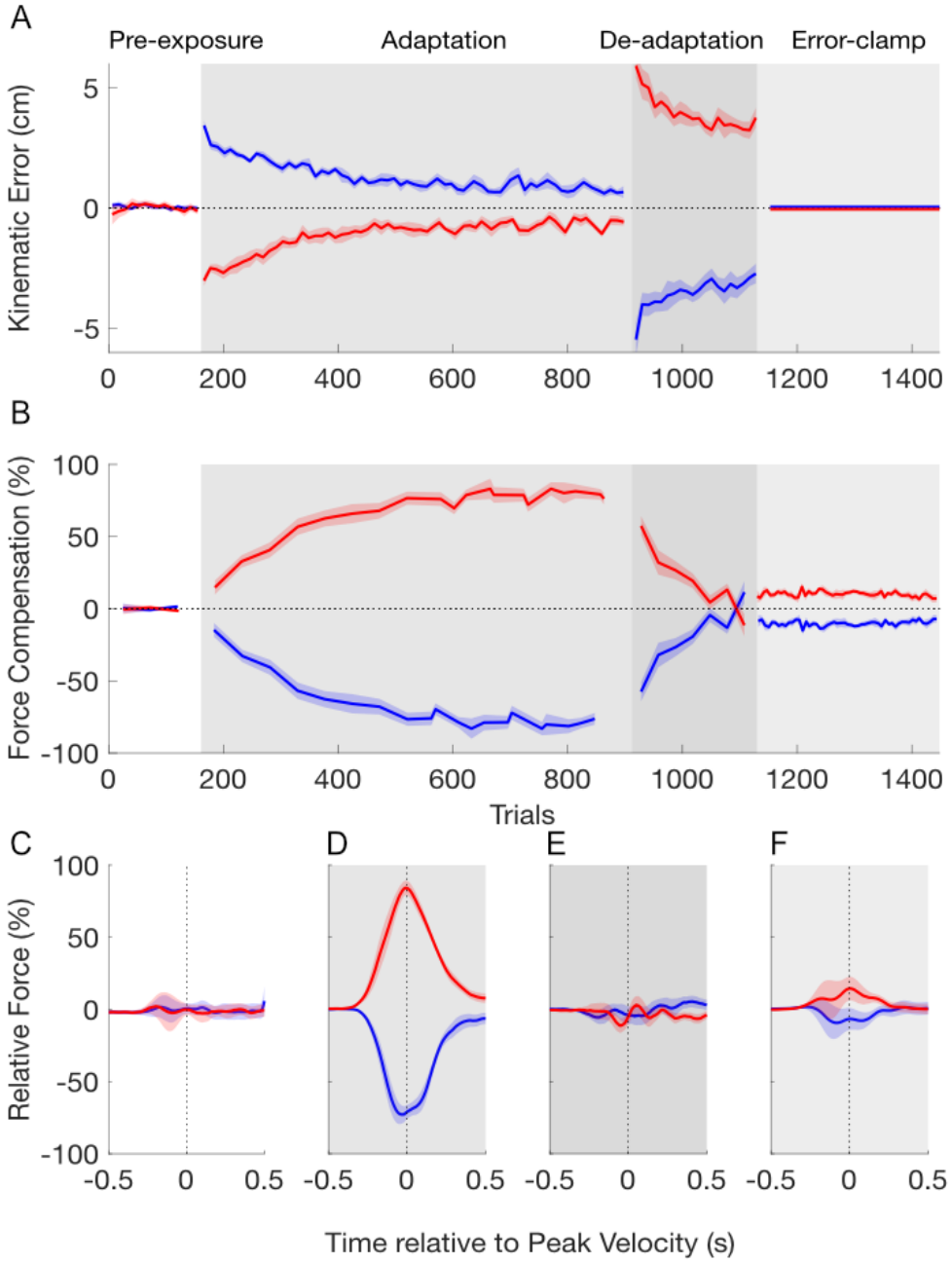

Figure 3. Temporal pattern of adaptation to opposing force fields in experiment 1. **A.** Mean of kinematic error over pre-exposure (white), adaptation (grey), de-adaptation (dark grey) and error-clamp (light grey) phases. The data of the contextual cue 1 (left visual workspace shift) and 2 (right visual workspace shift) are presented in red and blue lines, respectively. Shaded regions indicate the standard-error of the mean. **B.** Mean of force compensation. The force compensation for the two contextual cues is symmetrical due to the subtraction of the mean difference. **C.** Force profiles on the channel wall as a function of movement time in the pre-exposure phase. The force values are shown as a percentage of perfect force compensation and aligned to peak velocity. For each cue, the mean of force compensation is taken from all trials. **D.** Force profiles for the last 10 trials (blocks) in the adaptation phase. **E.** Force profiles for the last 3 trials (blocks) in the de-adaptation phase **F.** Force profiles for all trials in the error-clamp phase.

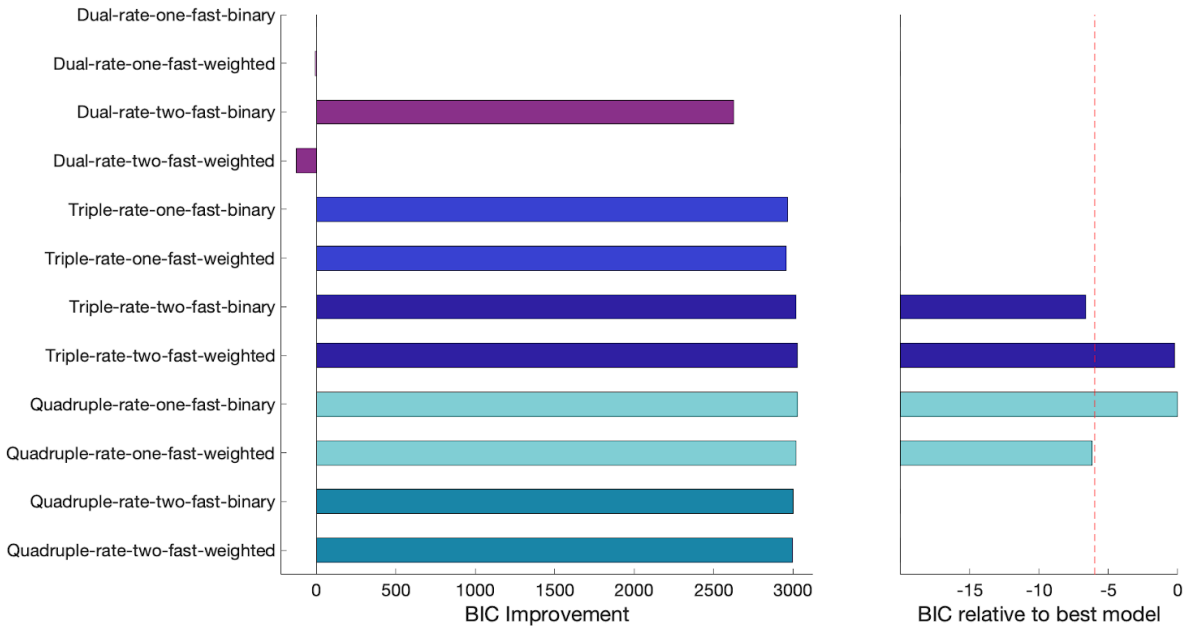

Figure 4. Bayesian Information criterion (BIC) model comparison for experiment 1. The twelve models are differentiated by their improvement in BIC relative to the referent model (value of 0, left). Improvements in BIC from 2 to 6, 6 to 10 and greater than 10 are considered as a positive, strong and very strong evidence any one model fitting better than the other models, respectively. On the right side, a zoomed in version of the best-fitting models is shown to see specific differences. The red line shows a BIC difference of 6 from the best-fitting model.

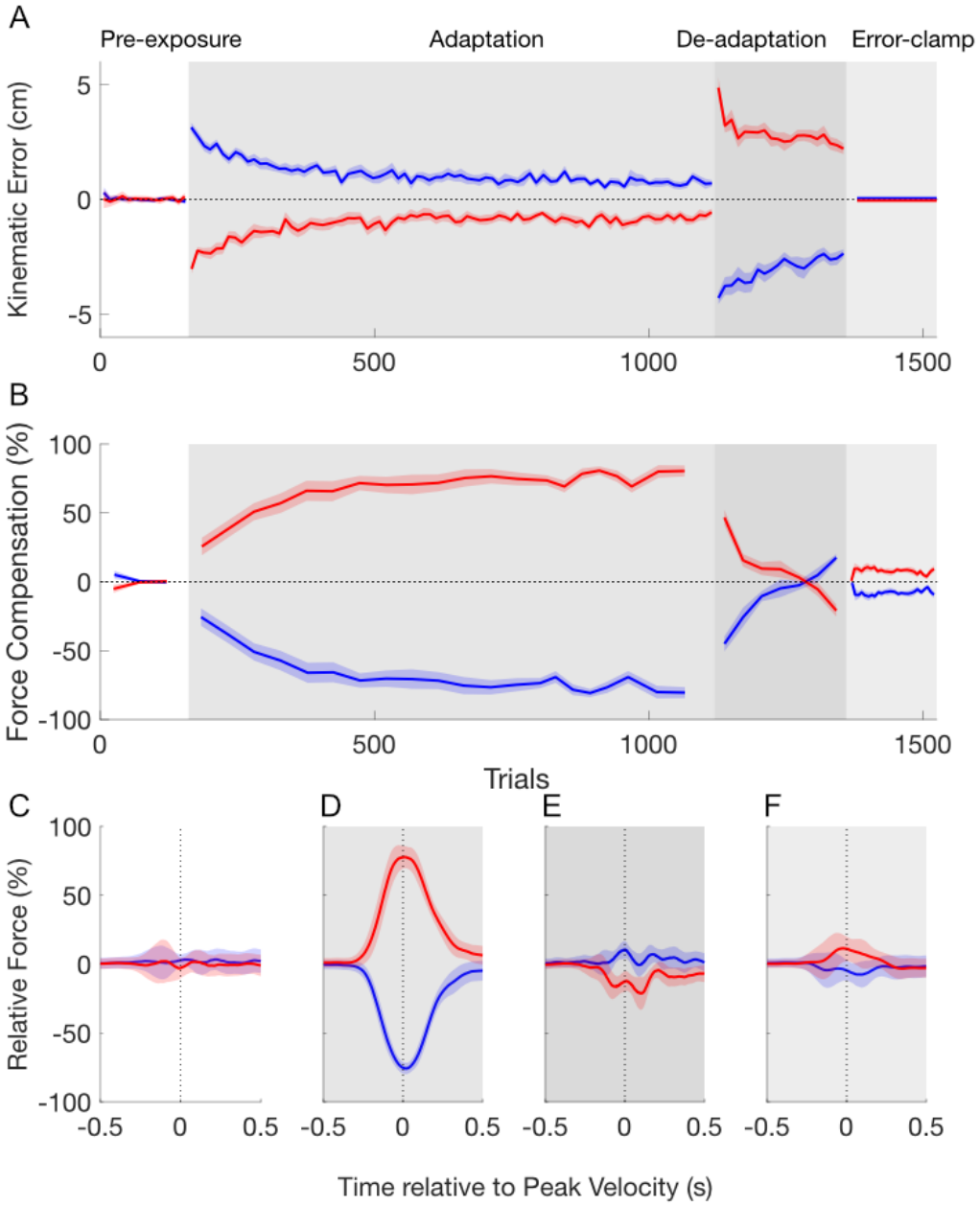

Figure 5. Temporal pattern of adaptation to opposing force fields in experiment 2. **A.** Mean of kinematic error over pre-exposure (white), adaptation (grey), de-adaptation (dark grey) and error-clamp (light grey) phases. **B.** Mean of force compensation. **C.** Force profiles on the channel wall as a function of movement time in the pre-exposure phase. **D.** Force profiles in the adaptation phase. **E.** Force profiles in the de-adaptation phase **F.** Force profiles for all trials in the error-clamp phase.

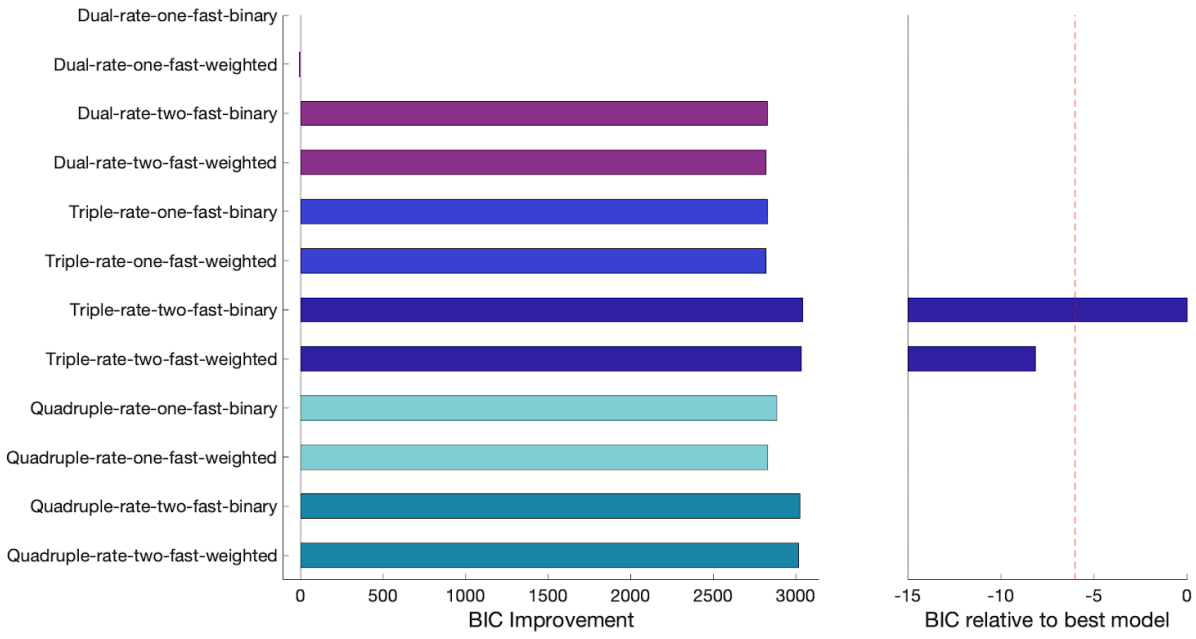

Figure 6. Bayesian Information criterion (BIC) model comparison for experiment 2.

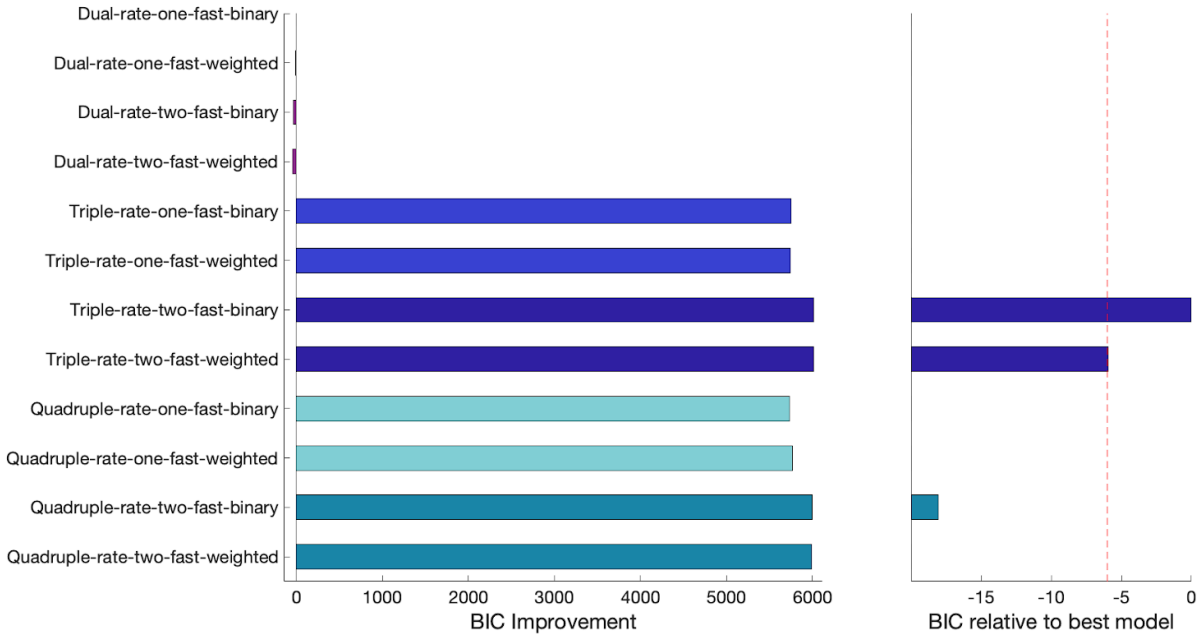

Figure 7. Bayesian Information criterion (BIC) model comparison across both experiments 1 and 2. Each model was fit simultaneously to the data from both experiments.

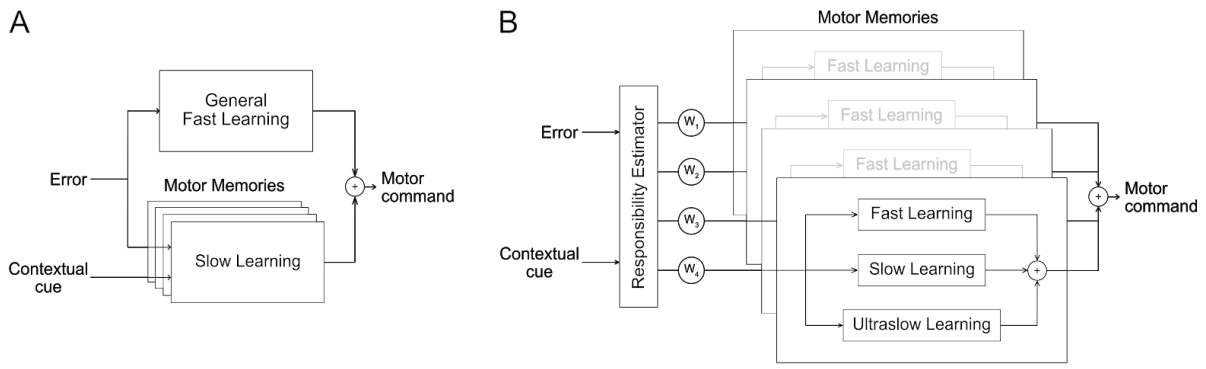

Figure 8. Models of motor learning. **A.** The dual-rate model with multiple slow processes acting in parallel and a single general fast process as proposed previously (Lee and Schweighofer, 2009). **B.** Our proposed model of adaptation consists of multiple parallel motor memories, each involving a fast, slow and ultraslow process, all weighted by a responsibility estimator.

Parameters		Retention rate				Learning rate				Switch
		Af	**As**	**Aus**	**Ahs**	**Bf**	**Bs**	**Bus**	**Bhs**	**c**
Triple	**binary**	0,631	0,992	1,000		0,137	0,007	0,003		
	weighted	0,655	0,992	1,000		0,148	0,008	0,004		0,920

Table 1. Parameters of the 2 fast triple rate models for either a binary or weighted contextual cue switch. The parameters were fit on the data from both experiments simultaneously.